The following publication A. Duan et al., "AuSoScan: Automatic Scoliosis Assessment by Ultrasound Scanning With Soft Contact Control," in IEEE/ASME Transactions on Mechatronics, vol. 30, no. 6, pp. 7693-7704, Dec. 2025 is available at https://doi.org/10.1109/TMECH.2025.3583041.

AuSoScan: Automatic Scoliosis Assessment by Ultrasound Scanning with Soft Contact Control

Anqing Duan, *Member, IEEE*, Wanli Liuchen, Peng Zhou, *Member, IEEE*, Dezhen Song, *Senior Member, IEEE*, Chenguang Yang, *Fellow, IEEE*, Yongping Zheng, *Senior Member, IEEE*, and David Navarro-Alarcon, *Senior Member, IEEE*

***Abstract*—In this paper, we present AuSoScan, a novel robotic platform that enables Automatic Scoliosis Assessment through ultrasound Scanning. Ultrasound imaging has been widely adopted in physical examinations due to its many benefits, such as being radiation-free, cost-effective, and highly portable. However, the scanning procedure is often tedious and labor-intensive, requiring sonographers to perform repetitive manual scanning tasks. With the fast development of robotic technologies in medical and healthcare applications, robotic ultrasound imaging presents a promising solution by combining the strengths of both robotic systems and ultrasonic devices. This has driven the development of AuSoScan, a platform specifically aimed at diagnosing scoliosis, a condition characterized by an abnormal lateral curvature of the spine. The hardware of the research platform consists of an ultrasound probe, a robotic arm, a depth camera, a force/torque sensor, and a workstation. The software architecture of the system comprises an ultrasonic perception model, a control system, and a 3D spinal image reconstruction program. The control system of AuSoScan is implemented using model predictive control (MPC), explicitly accounting for the soft contact between the ultrasound probe and the patient's back to enable precise force control. The effectiveness of AuSoScan is evaluated by real-world experiments of assessing the scoliosis on a phantom.**

***Index Terms*—Medical robots and systems, robotic ultrasound imaging, force control, image processing, healthcare robotics.**

I. Introduction

SCOLIOSIS refers to an abnormal lateral curvature of the spine [1]. Common patterns of scoliosis include thoracic, lumbar, thoracolumbar, or combined thoracic and lumbar scoliosis, as illustrated in Fig. 1. It is the most common spinal deformity with a prevalence of approximately 470 to $5,200$ per $100,000$ individuals worldwide [2]. Scoliosis brings several negative effects to the patients, such as psychosocial disability, mechanical pulmonary restriction, and even back pain. The scoliosis progression requires close and frequent monitoring because timely intervention usually ensures the best therapeutic effect.

As a gold standard for scoliosis assessment, the Cobb's angle method has been widely used to quantify the severity of spinal deformities since its invention [3]. The Cobb angle is defined as the angle between the upper border of the uppermost vertebra and the lower border of the lowermost vertebra in the coronal plane, representing the lateral deviation of the spine. Despite its popularity, the Cobb angle approach to scoliosis assessment has certain risks and drawbacks. One significant deficiency is the exposure to radioactive X-rays, as it is measured based on a posterior-anterior radiograph. Since the monitoring of the scoliosis progression of a child has to be performed every four to six months throughout adolescence [4], it is always worrisome that repeated exposure to radiographs would increase the risk of future iatrogenic cancer risks for children [5]. Recent studies show that the cancer rate developed in a cohort of adolescent idiopathic scoliosis patients is five times higher than the age-matched population, which calls for the reduction of the radiation dose [6].

Considering the dangerous ionizing radiation caused by X-rays, the development of a radiation-free alternative is imperative. In particular, sonography serves as a popular technique in medical health diagnosis because it is radiation-free, low-cost, and widely accessible [7]. Although long thought to be effective only for imaging soft tissues of the body, the feasibility of ultrasound imaging bones such as spines has recently been demonstrated, thus providing a new method for assessing scoliosis [8]. A comparison between radiography and sonography is shown in Figs. 1 (e) and (f).

Building upon the promising advancements in diagnosing scoliosis using ultrasonography, this paper focuses on automating the scanning procedure. Currently, in manual spinal scanning, a sonographer applies pressure to an ultrasound probe and slides it in a posterior-anterior direction to track the center of the vertebrae, specifically the spinous process [9]. Our objective is to perform ultrasonic spine scanning using a robotic manipulator instead of relying on a human sonographer. We believe that the autonomous acquisition of ultrasound images has many benefits. Firstly, it relieves sonographers from the tedious and repetitive task of manual scanning [10]. Secondly, patients can receive a more standardized treatment at a more affordable cost for examination. In addition, robotic-assisted medical checks offer a promising solution to address the problem of medical personnel shortage.

This research is funded in part by the Research Impact Fund of the HK Research Grants Council under grant R5017-18F, in part by PolyU through the Intra-Faculty Interdisciplinary Project under grant ZVVR, and in part by PolyU under grant G-UANS. (*Corresponding author: David Navarro-Alarcon.*)

Anqing Duan and Dezhen Song are with the Mohamed bin Zayed University of Artificial Intelligence (MBZUAI), Abu Dhabi, United Arab Emirates (e-mail: anqing.duan@mbzuai.ac.ae; dezhen.song@mbzuai.ac.ae).

Peng Zhou is with the School of Advanced Engineering, The Great Bay University, Dongguan, China (e-mail: pzhou@gbu.edu.cn).

Chenguang Yang is with Department of Computer Science, University of Liverpool, Liverpool, L69 3BX, U.K. (e-mail: cyang@ieee.org)

Wanli Liuchen, Yongping Zheng, and David Navarro-Alarcon are with The Hong Kong Polytechnic University (PolyU), KLN, Hong Kong (e-mail: cwanli.liu@polyu.edu.hk; yongping.zheng@polyu.edu.hk; dna@ieee.org).

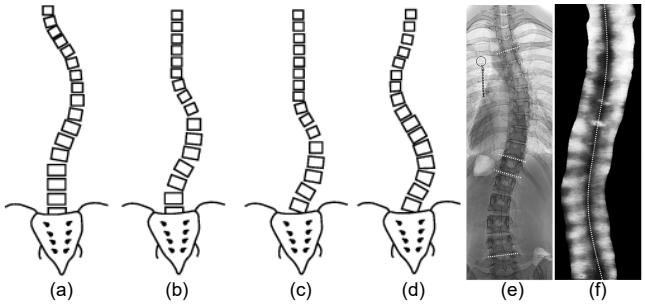

Fig. 1. Illustration of different patterns of scoliosis, including (a) Thoracic curve, (b) Thoracolumbar curve, (c) Lumbar curve, and (d) Double major curve as well as the imaging of spines in (e) Radiography and (f) Sonography for scoliosis assessment.

Formally, we present AuSoScan, a novel robotic platform that enables **Au**tomatic **Sco**liosis assessment by ultrasound **Scan**ning. AuSoScan automates the coronal spine image acquisition process. AuSoScan employs a robotic manipulator to replace the human sonographer. The end-effector of the robot arm is equipped with an ultrasound probe that is used for ultrasound imaging as in the manual case. The control system design of AuSoScan employs a model-predictive approach. This predictive controller takes the signals from the ultrasonic transducer as input and generates the optimal control commands. Moreover, the proposed controller explicitly accounts for the soft contact between the ultrasound probe and human back tissue and skin. The 3D spinal image is then reconstructed from the ultrasound images captured by the robotic scanning [11].

To summarize, the original contributions of this paper are outlined as follows:

- Development of an innovative robotic scanning system, which integrates a robot arm with an ultrasound probe, to realize automatic ultrasonic spine scanning;
- Implementation of a novel control system, which generates control signals by perceiving ultrasound images whilst taking soft probe-tissue contact into account.

The remainder of the paper is organized as follows. First, related work is reviewed in Sec. II. The hardware set-up is introduced in Sec. III and the software development is presented in Sec. IV. The effectiveness of AuSoScan is evaluated in Sec. V. Finally, Sec. VI concludes this paper.

II. Related Work

Robot-Assisted Sonography: Robotic ultrasound imaging, an interdisciplinary field that merges robotics and ultrasonography, has garnered significant interest. The development of autonomous imaging is at the forefront of this field, promising to minimize human involvement. To achieve autonomous scanning, a multimodal deep reinforcement learning model that integrates visual and tactile information is utilized to determine the ultrasound probe's pose [12]. Additionally, deep reinforcement learning is applied to identify high-quality standard planes from volumetric ultrasound data [13]. Besides, Bayesian optimization is employed to adjust the scanning angle during thyroid imaging [14]. Our approach is distinguished from the previous studies in terms of its focus on the modelling of the soft contact between the human skin and the ultrasound probe. Thanks to an explicit deformation model, our method enables reliable and effective control of the soft interaction with the ultrasound probe.

Ultrasonic Perception: Compared to the traditional visual servoing strategy, which aims to synthesize a robot's motion based on visual features [15], the processing of spinal ultrasound images for real-time robot control is more complex. Challenges primarily arise from two sources: inherent speckle noise and image quality evaluation. The presence of inherent speckle noises prevents us from straightforward identification of desired anatomical attributes [16]. In conventional ultrasound image processing techniques, a pre-processing step is typically employed to denoise raw images. For instance, in the case of determining a needle insertion site, support vector machines with Gaussian kernels are applied to denoised ultrasound images to classify spinous process images and interspinous images [17]. By contrast, in our work, the objective is for the ultrasonic perception module to localize the region of interest, specifically the spinous process, rather than classifying it. It is worth mentioning that a random walk-based confidence map is commonly used [18] in ultrasound image evaluation. Although this approach achieves promising results when evaluating the quality of ultrasound images of soft tissues, the same principle may not be suitable for evaluating ultrasound images of bones. Our ResNet-based ultrasonic module can effectively overcome these limitations [19].

Soft Contact Mechanics: The contact established between the probe and the large posterior area of the human body constitutes a soft interaction [20], which represents a unique challenge compared with non-contact applications [21], [22]. While rigid contact has been extensively studied in various grasping and manipulation applications [23], soft interaction has also received significant attention in areas such as needle insertion [24], suturing [25], and cutting [26]. In our application, we specifically focus on hybrid motion/force control on a soft substrate. Typically, a second-order mass-damping-spring model is employed to describe the contact dynamics behavior [27]. However, in this paper, we propose building the soft contact dynamics model using the Hertzian theory, as suggested by [28] in the context of soft spherical interactions. Compared to the work by [28], we instead investigate the cylinder-plane interaction, as the shape of the cylinder better represents the geometry of the probe than a sphere. Moreover, we explicitly consider the resistance force caused by deformation in our model.

III. Hardware Design

In this section, we will introduce the overall hardware system of AuSoScan, which is built on top of the Scolioscan system, a 3D ultrasound imaging platform for manual scoliosis assessment [29]. We first briefly introduce the Scolioscan system in Sec. III-A. Subsequently, we introduce the hardware components of AuSoScan in Sec. III-B.

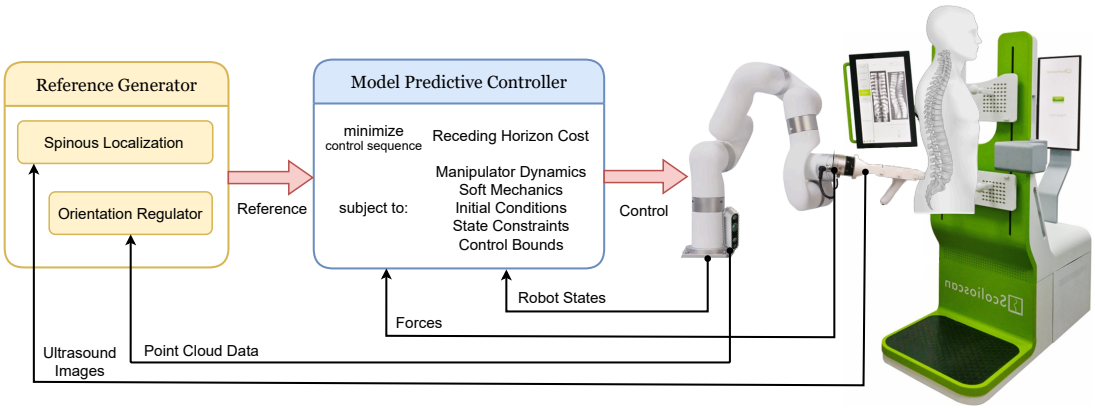

Fig. 2. Illustration of the developed control system for AuSoScan, which is devised based on the model predictive control with the incorporation of the proposed soft contact model. The model predictive controller minimizes the tracking cost over a sequence of control signals while satisfying a set of constraints, including manipulator dynamics, soft contact mechanics, as well as state and control bounds. In addition, the tracking objective is provided by the reference generator, which is responsible for localizing the spinous process and providing back surface normal vectors.

A. Scolioscan Platform

The Scolioscan system (Model SCN801, Telefield Medical Imaging Ltd, Hong Kong), endowed with commercial and ergonomic designs, was previously developed for 3D ultrasound imaging of spines to enable scoliosis assessment [29]. The usage of Scolioscan can be characterized by the following three phases, namely pre-, intra-, and post-scanning.

Before starting a scan, the patient is instructed to stand on the podium equipped with an anti-fatigue mat. The patient's anterior concave border of the clavicle and anterior superior iliac spine is supported by the chest and hip supporting boards, respectively. Two supporting pillars are installed on each supporting board to compensate for the potential body displacement caused by the probe's pressure. Both the supporting boards and the supporting pillars are adjustable according to the patient's height. The scanning range is then determined by recording the lower and upper boundaries using the ultrasound probe. The customized probe runs at a frequency of $4-10\,\mathrm{MHz}$ with a width of $10\,\mathrm{cm}$.

During the scanning procedure, a sonographer performs steady freehand scanning from the fifth lumbar vertebra to the first thoracic vertebra. The scanning process is facilitated by two LCD screens, providing information to both the patient and the sonographer. The front touch screen guides the sonographer's scanning movements, while the other screen provides an evaluation procedure for the patient. To ensure a stable posture for the head and neck during scanning, the patient is instructed to focus on a green eye spot. The location of the eye spot is adjusted based on the patient's height. The electromagnetic spatial sensor measures the position and orientation of the probe, and it communicates with an onboard electromagnetic transmitter located inside the transmitter box.

After the completion of scanning, the recorded B-mode ultrasound images, along with the corresponding spatial information collected from the probe, are utilized for the 3D reconstruction of the patient's spine. Finally, the sonographer performs the analysis of the coronal view of the image for scoliosis examination.

B. Robotic Hardware

In this section, we present the specifications of the hardware system of AuSoScan. Being an automated version of Scolioscan, AuSoScan aims to achieve the scanning task automatically using a robotic manipulator, thus eliminating the need for a sonographer. The hardware components and their respective responsibilities are described in detail below.

The key component of AuSoScan is the UFACTORY xArm 6, a collaborative robotic arm. The xArm is a serial robot manipulator equipped with six degrees of freedom (DoFs). The base of the robot arm is mounted on a wheeled supporting platform. During the preparation phase of a scanning task, the supporting platform is positioned in a way that ensures the entire back of the patient falls within the robot arm's working space. To maintain stability, the wheels of the supporting platform are locked before activating the control box of the robot arm. For communication, the xArm robot manipulator is connected to a workstation using the TCP/IP protocol, operating at a rate of $125\,\mathrm{Hz}$.

AuSoScan is designed to be able to sense and perceive the environment and manipulate the ultrasound probe as the end effector in response to the sensory feedback in real time like a human sonographer. To achieve such advanced and sophisticated sensorimotor control, the sensing and perception system of AuSoScan incorporates multiple sensors, including an ultrasonic transducer, an F/T sensor, and a depth camera.

The ultrasound probe used in AuSoScan is Scolioscan SCN201, which is a palm-sized portable ultrasonic transducer. Scolioscan SCN201 is crafted to be ultra-light with a net weight of $500\,\mathrm{g}$ and has a suitcase dimension of $182\times97\times150\,\mathrm{mm}$. The probe is mounted on the last link of the robot arm by being clamped by a customized 3D-printed fixture. The probe captures the spinal ultrasound images at a frequency of $7.5\,\mathrm{MHz}$ and sends raw ultrasonic data at a frame rate of $10\,\mathrm{fps}$ to the workstation. The relatively low frame rate necessitates the robot moving slowly along the subject's back to ensure reliable control. The aperture of the probe has a rectangular shape with an acoustic transducer length of $80\,\mathrm{mm}$ and width $15\,\mathrm{mm}$. The transmitted ultrasound images are organized with

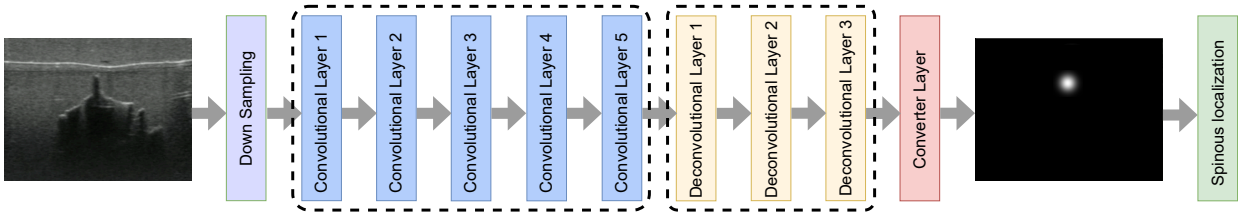

Fig. 3. Illustration of the pipeline for spinous process localization. The raw ultrasound image is first down-sampled and then fed into the ultrasound perception neural network, whose output is a heatmap image with the maximum intensity indicating the detected spinous process.

a size of 640×480 pixels.

To monitor the contact forces between the human back and the ultrasound probe for reliable physical interactions, a six-axis Force/Torque sensor Robotiq FT300 is installed between the ultrasound probe and the robot arm end-effector. The F/T sensor works at a sampling frequency of $1\,\mathrm{kHz}$. With the measured force value by the F/T sensor, it becomes feasible to implement a direct force control strategy as presented in the next section.

To ensure stable acoustic coupling during the scanning procedure, it is important to handle the ultrasound probe, guaranteeing its tip consistently points toward the human back and maintains contact. This requires knowledge of the normal vectors of the human back. To fulfill the requirement, we integrate a RealSense depth camera into AuSoScan. The depth camera is positioned at the base of the robot manipulator. Before automatic scanning, the depth camera is used to sense the human back and retrieve the normal vectors.

Additionally, we include a scoliosis phantom in the AuSoScan platform. The phantom contains a scoliotic spine sealed inside its upper body. The skin surface of the phantom is made from agar, which is a common material for mimicking human skin. The stiffness of the phantom has been previously identified, which is similar to that of human skin [30]. The realistic phantom facilitates in vitro studies of the robotic scanning, and the results will also be informative and applicable to scenarios involving the human body. The overall scanning procedure operates as follows. Before the formal scanning starts, the RealSense camera first captures the subject's back to obtain normal vectors. Next, the probe is extended to make contact with the human back. Once contact is established, the robot arm moves upward to track the spinous processes, guided by the position provided by the ultrasound perception network.

IV. Software Development

In this section, we describe the individual software components of AuSoScan, which include the ultrasonic perception module (IV-A), the robot control system (IV-B), and the spinal reconstruction program (IV-C).

A. Ultrasonic Perception Module

The ultrasonic perception module is responsible for the real-time processing of raw ultrasound images, with the objective of extracting and transmitting the position of the spinous process to the subsequent robot control system. The accurate detection of the spinous process is crucial for the success of spinal reconstruction. To enhance the detection of the spinous process, we propose the utilization of the widely adopted heatmap approach. This approach involves generating a heatmap image that reflects the probability of each pixel in the original ultrasound image belonging to the spinous process. In essence, the heatmap provides a visual representation of the spinous process position, with the pixel exhibiting the highest intensity indicating its location.

To transform an ultrasound image into a heatmap image, we build our ultrasonic perception network based on the ResNet since it is widely used for image processing tasks like key feature identification. As a backbone of our perception network, ResNet extracts the image features from input ultrasound images through five convolutional stages. Then, a decoder is designed to map the image features to heatmaps. To this end, the last fully connected layer of the original ResNet structure is modified by three deconvolutional layers that have batch normalization and ReLU activation. There are 256 filters for each deconvolutional layer. Furthermore, the size of the kernel is 4×4 and the stride step is 2. Finally, to output a heatmap, which is organized in a size of 56×56, the deconvolutional layers are augmented by a 1×1 convolutional layer.

The dataset for training the ultrasonic perception network consists of a set of paired ultrasound images as input and heatmap images as output. To collect ultrasound images, a total of 25 test subjects with scoliosis are involved[1]. Among them, 7 subjects have moderate scoliosis, namely, spinal deformity angle ranging from 25° to 37°, and the remaining 18 subjects have mild scoliosis, namely, spinal deformity angle ranging from 10° to 24°. The input ultrasound images are collected by manually scanning the test subjects. There are a total of $13,674$ spinous process images in the dataset, containing 425 spinous processes with 17 spinous processes for each subject. The corresponding output heatmap images are generated from each ultrasound image by labeling its spinous process location and forming a 2D Gaussian distribution in accordance with the label's center.

The loss function for training the ultrasonic perception network is defined with the mean squared error. Given an ultrasound image I_n and its corresponding heatmap output H_n^*, the loss function is expressed by

$$\mathcal{L}(\theta) = \frac{1}{N} \sum_{n=1}^{N} \left\| H_\theta(I_n) - H_n^* \right\|^2, \tag{1}$$

[1]Ethical approval HSEARS20210417002 was granted by the Departmental Research Committee on behalf of PolyU Institutional Review Board.

where θ denotes the parameters to be learned for the neural network and N represents the total number of training data points. In addition, the five-fold cross-validation for human subjects is employed so that the images from the same subject do not appear in the training and testing datasets at the same time. To increase the robustness of the dataset, several data augmentation methods are randomly selected for each image, including image rotation, translation, and flipping.

B. Control System

The primary objective of the control system of AuSoScan is to drive the robotic arm in tracking the spinous processes, ensuring that their position remains centered within the ultrasonic window. Our control system is built using a Model Predictive Control (MPC) approach, which provides a general and flexible framework for controller design [31].

In brief, MPC iteratively solves an online optimization problem in search of the optimal control action that drives the system states based on a predefined cost function. Formally, the template of MPC is formulated as follows

$$\begin{aligned}
\min_{\{u_k\}_{k=0}^{l-1}} \quad & \sum_{k=0}^{l-1} \phi(x_k, u_k) + \psi(x_l) && \text{(2a)}\\
\text{s.t.} \quad & x_{k+1} = \mathcal{F}(x_k, u_k), && \text{(2b)}\\
& x_0 = x_{\texttt{current}}, && \text{(2c)}\\
& x_k \in \mathcal{X}, && \text{(2d)}\\
& u_k \in \mathcal{U}, && \text{(2e)}\\
& \forall k = 0, \ldots, l-1.
\end{aligned}$$

The control objective is expressed in (2a) where ϕ denotes the tracking cost and ψ denotes the terminal cost. The constraints of MPC need to be satisfied over the horizon length l, which encompass system dynamics (2b), and feasible regions of states (2d) and controls (2e). Each iteration of MPC is initialized with the current measured states (2c). By iteratively solving the optimization problem at every control step, the optimal control sequence can be derived, with the first one u_0 being actually executed.

In what follows, we elaborate on the instantiation of the MPC template provided in (2) toward our application scenario. First of all, we consider the determination of the set of states of AuSoScan's control system. For robot arm control, the generalized position vector q and velocity vector $\dot{q}$ are chosen as the system states. In addition, we would like to achieve direct force control to regulate the interaction between the ultrasound probe and the human body, which is usually enabled by the closure of a force feedback loop. To this end, the interaction force F is also incorporated as a controlled variable. Consequently, the system states x are compactly expressed as

$$x = \begin{bmatrix} q^\intercal & \dot{q}^\intercal & F^\intercal \end{bmatrix}^\intercal. \tag{3}$$

The control signals of the MPC controller u are chosen as the robot joint torques τ, namely

$$u = \tau. \tag{4}$$

Subsequently, we consider the modeling of the system dynamics. The full system dynamics are composed of two parts: manipulator dynamics and soft interaction dynamics. The model for manipulator dynamics is given by:

$$\ddot{q} = M(q)^{-1} \left(\tau - C(q, \dot{q})\dot{q} - G(q) - J(q)^\intercal F \right), \tag{5}$$

where $M(q)$ is the mass matrix, $C(q, \dot{q})$ is the Coriolis matrix, $G(q)$ is the gravity term, and $J(q)$ is the Jacobian matrix.

In addition to the manipulator dynamics, it is necessary to account for the contact dynamics, as the interaction force is considered part of the system states. Typically, there are two primary types of robot-environment interaction: rigid contact and soft contact [32]. The former is featured by the constraints of robot motion due to the establishment of contact with the rigid environment, leading to the degeneration of the robot's degree of freedom. The latter deals with the interaction dynamics prescribed by the fundamental physical effects, such as inertia, elasticity, and dissipation.

Since the human body consists of soft tissues, the interaction dynamics are thus categorized as soft contact. Traditionally, contact models for soft tissues are constructed using linear rheological elements, such as parallel and/or serial combinations of linear springs and linear dampers [33]. These viscoelastic models are particularly appropriate for studying system behavior in the direction of penetration. However, in our scenario, the robot end-effector is intended to slide on the surface of the soft tissues rather than penetrate them. Consequently, it is crucial to explicitly model the deformation of the contact surface to facilitate the derivation of the soft contact dynamics.

We propose to model the soft contact dynamics by resorting to the Hertzian contact theory, a popular tool in the field of tribology and contact mechanics [34]. Compared to the simpler spring-damper system for soft contact modeling, our approach, based on Hertzian contact theory, offers several advantages. Firstly, our specific application, which involves sliding over a soft surface, requires understanding the geometric properties of the local deformation region. These properties are readily derived from Hertzian theory, unlike spring-damper modeling. Secondly, Hertzian theory allows for the incorporation of material properties such as Young's modulus and Poisson's ratio, offering a more precise characterization of deformable contacts.

Our objective is to establish a relationship between the contact forces and the kinematic motion of the robot arm. In particular, we focus on modeling the forces along the normal and moving directions, as these force components play a significant role in determining the contact dynamics.

We first review the contact surface deformation under static contact, i.e., the relative speed between two contact objects is zero. We assume the geometric shape of the probe is a cylinder, and the human back surface is flat. For static contact, the Hertzian pressure distribution as a function of distance from the center of the pressed circle is given by

$$p(r) = p_s \left(1 - \frac{r^2}{a^2} \right)^{1/2}, \tag{6}$$

where p_s denotes the maximum pressure and a denotes the radius of the contact circle. The expression for the maximum pressure value with respect to the indentation d and the equivalent radius R is given by

$$p_s = \frac{E^*}{2}\sqrt{d/R}. \tag{7}$$

The elastic property E^* is defined by

$$\frac{1}{E^*} = \frac{1-\nu_1^2}{E_1} + \frac{1-\nu_2^2}{E_2}, \tag{8}$$

where E_1 and E_2 are Young's moduli of elasticity, and ν_1 and ν_2 are the Poisson's ratios of the human back and the ultrasound probe, respectively. As the ultrasound probe is made from rigid materials, we approximate its modulus of elasticity E_2 as infinity. As a result, it leads to

$$E^* = E_1/(1-\nu_1^2). \tag{9}$$

The equivalent radius R is defined by

$$\frac{1}{R} = \frac{1}{R_1} + \frac{1}{R_2}, \tag{10}$$

where R_1 and R_2 represent the radius of the human back and the ultrasound probe, respectively. Here we treat the human and phantom back as a flat surface, which is a common strategy in deformation modeling [28]. As a result, the radius R_1 goes to infinity, which leads to $R = R_2$.

During the scanning procedure, the deformation of the contact surface is not static. Specifically, due to the relative motion between the human back surface and the ultrasound probe, the deformation shape of the surface is distorted by the probe's motion, as shown in Fig. 4. Due to the relative motion, the contact region at the front of the probe will be increased, and the contact point at the rear of the probe will be decreased compared with the static case. As a result, we propose to modify the static pressure distribution as follows:

$$p(r) = \begin{cases} p_m\left(1-\dfrac{r^2}{a_1^2}\right)^{1/2} & -a_1 \le r \le 0, \\ p_m\left(1-\dfrac{r^2}{a_2^2}\right)^{1/2} & 0 < r \le a_2, \end{cases} \tag{11}$$

where we still assume a similar shape of stress distribution while the front radius and the rear radius become a_1 and a_2, respectively, and p_m denotes the maximum pressure. Here we focus on the radius change with respect to the static contact under the same normal strength F. Assuming that the change of the deformation radius locally remains a linear relationship with respect to the moving velocity v, we then have the front radius and the rear radius to be

$$a_1 = \sqrt{Rd_0} - k_1 v \quad \text{and} \quad a_2 = \sqrt{Rd_0} + k_2 v, \tag{12}$$

where k_1 and k_2 denote the linear coefficients and d_0 represents the static penetration depth given by

$$d_0 = 4F/(\pi E^* L). \tag{13}$$

Here, L is the width of the ultrasound probe.

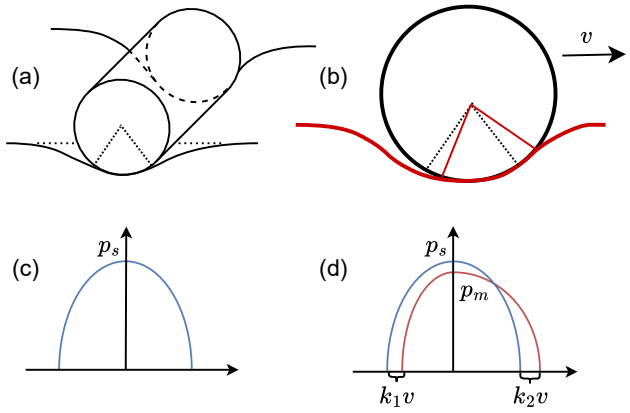

Fig. 4. Illustration of surface deformation. (a) Static case. (b) Relative sliding. (c) Static stress distribution. (d) Sliding stress distribution.

Our goal is to express the normal force F with respect to the dynamic penetration d. To this end, we first have the normal force by integrating the stress distribution:

$$\begin{aligned} F &= \int_0^L \int_{-a_1}^{a_2} p(r)\, dr dl = \frac{\pi L p_m}{4}(a_1 + a_2) \\ &= \frac{\pi L p_m}{4}\left(2\sqrt{Rd_0} + \Delta k v\right), \end{aligned} \tag{14}$$

where we define $\Delta k = k_2 - k_1$. Provided the maximum pressure is determined only by the indentation depth, by substituting (7) into (14), we finally obtain the relationship between the normal force and the penetration depth as

$$F = \frac{\pi L E^*}{8}\left(2\sqrt{Rd_0} + \Delta k v\right)\sqrt{d/R}. \tag{15}$$

Regarding the friction along the probe's moving direction, we identify that there are two factors that contribute to the frictional effects: dry friction f_d between the moving surfaces and internal friction f_b caused by surface deformation. The overall friction is obtained by the superposition of these two effects, namely $f = f_d + f_b$ where $f_d = \mu F$ with μ representing the kinetic friction coefficient. Furthermore, the internal friction f_b is obtained by calculating the following integral

$$\begin{aligned} f_b &= \int_0^L \int_{-a_1}^{a_2} \frac{rP(r)}{\sqrt{R^2 - r^2}}\, dr dl \\ &= \int_0^L \int_{-a_1}^{0} \frac{P_m r}{a_1}\sqrt{\frac{a_1^2 - r^2}{R^2 - r^2}}\, dr dl + \\ &\qquad \int_0^L \int_0^{a_2} \frac{P_m r}{a_2}\sqrt{\frac{a_2^2 - r^2}{R^2 - r^2}}\, dr dl \end{aligned} \tag{16}$$

where we insert the pressure distribution in (11).

The interaction dynamics model can be obtained by calculating the derivatives of (15) and (16). The dynamics model for the normal force is given by

$$\dot{F} = \frac{\pi L E^* \Delta k}{8}\left(\dot{v}\sqrt{\frac{d}{R}} + \frac{v\dot{d}}{2\sqrt{Rd}}\right). \tag{17}$$

The model for friction dynamics is directly obtained by calculating the derivative of f:

$$\dot{f} = \mu \dot{F} + \dot{f}_b. \tag{18}$$

The control objective of MPC is designed by specifying the cost function, whose minimization ensures that the trajectory of the states can be steered toward the desired system behavior. The overall cost function is formulated by a weighted linear combination as

$$\phi = w_1 \phi_{\texttt{config}} + w_2 \phi_{\texttt{pose}} + w_3 \phi_{\texttt{force}} + w_4 \phi_{\texttt{energy}} \tag{19}$$

where $\phi_{\texttt{config}}$ denotes the joints configuration tracking cost; $\phi_{\texttt{pose}}$ denotes the end-effector pose tracking cost; $\phi_{\texttt{force}}$ denotes the interaction force tracking cost, and $\phi_{\texttt{energy}}$ denotes the control efforts cost, with w_1, w_2, w_3, and w_4 being the corresponding weights.

Moreover, the hardware-related constraints can be readily prescribed in the MPC controller. The robot joint position constraints and velocity constraints are written as $q \in \begin{bmatrix} q_{\min} & q_{\max} \end{bmatrix}$ and $\dot{q} \in \begin{bmatrix} \dot{q}_{\min} & \dot{q}_{\max} \end{bmatrix}$. The system's control constraints as a result of joint torque limitation are expressed as $u \in \begin{bmatrix} \tau_{\min} & \tau_{\max} \end{bmatrix}$.

C. Spinal Reconstruction Program

Once the scanning is finished, the acquired ultrasound image frames are then used for 3D reconstruction of the spine. Here we employ the volume projection imaging method for spinal reconstruction [35]. The procedure of volume projection imaging mainly consists of two main steps: 1) Build volume data, and 2) Slice for coronal view.

To build volume data, the collected ultrasound image frames are first concatenated layer by layer in reference to the associated corresponding spatial information obtained by the spatial sensors, as shown in Fig 5. Due to the inconsistency of the scanning intensity, the obtained raw 3D data needs to be further processed to generate volume data. Specifically, each voxel of the 3D image is obtained by interpolation of the 3D data points. For a compromise between computation speed and image quality, the rule of squared inverse weighted interpolation is employed, which assigns the relative weight for the k-th pixel as $W_k = 1/(d_k + \alpha)^2$, where d_k denotes the distance of the k-th pixel to the concerned voxel and $\alpha > 0$ is a hyperparameter that controls the effect range of the interpolation. More precisely, when α is chosen to be large, the speckles will be restrained and the image will be blurred. On the other hand, when α is chosen to be small, the texture pattern will be distinguishable, and the image tends to be noisy.

Once the interpolation is performed, the volume data will be subject to slicing for coronal view visualization. Though a 2D projection image is conventionally generated by planar volume rendering, the same slicing strategy is not feasible in our case of spinal rendering, as human spines have a specific non-planar curve shape. A planar slice of the volume data will result in information loss, i.e., some spinal features will be absent from the 2D projection image. To convey the spinal information on the rendered 2D image as much as possible, a more thoughtful slice strategy than a planar slide is necessary.

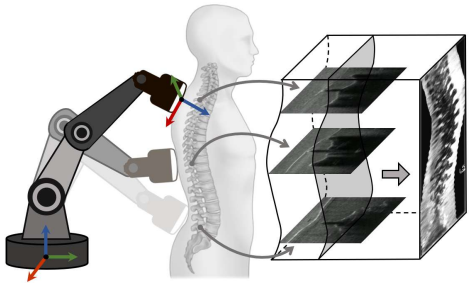

Fig. 5. Schematic illustration of Volume Projection Imaging for the acquisition of the ultrasound image of a spine.

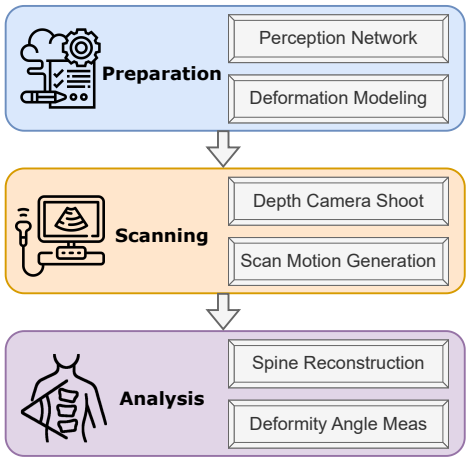

Fig. 6. Working flowchart of the overall automatic scanning. The procedure begins by training the ultrasonic perception network and identifying the model for soft contact. Then, the robotic system detects the geometry of the subject's back and generates the scanning motions. Finally, the spine is reconstructed, and the deformity angle is measured.

To take the natural pattern of the spine into account while making the slice, a non-planar developable surface is determined. The developable surface is used for volume rendering with consideration of the natural curve of the spine. To this end, a profile surface, which refers to the shape of spine volume data, is automatically identified from the volume data by discerning the first non-void voxels from a skin-to-spine direction. Then, the developable surface is determined by shifting the profile surface with a relative disposition. Finally, a number of adjacent surfaces of the developable surface are selected to include the hidden information about the spine by fusing different layers. The final rendering image is generated by a blending function of average intensity compounding.

A schematic diagram of the overall working flow of AuSoScan is illustrated in Fig. 6.

V. Experiments

In this section, we evaluate the effectiveness of AuSoScan with real experimental studies. The experimental studies are conducted module by module. We first showcase the effectiveness of the ultrasonic module. Subsequently, we test the control strategy of position and force control in the presence of soft interaction. Lastly, we perform ultrasonic scanning for real scoliosis assessment.

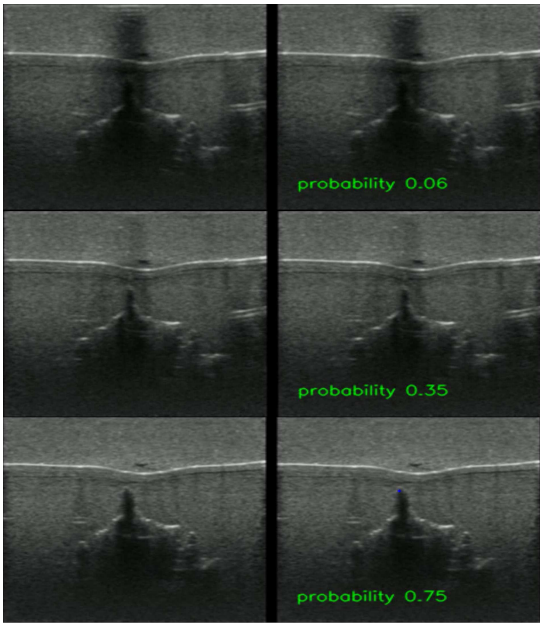

Fig. 7. Different confidence probabilities of identifying the spinous process in the lumbar region.

A. Ultrasonic Perception

The role of the ultrasonic module is to perceive the ultrasound images of the spines. In particular, the region of interest is the spinous processes. The robot arm tracks the position of the spinous process such that it is maintained in the center of the ultrasound image window. The ultrasonic perception network is devised by taking ultrasound images as input and output the confidence on the position of the spinous process. The ultrasonic perception network is trained with the Adam optimizer at a learning rate of 0.0001.

We evaluate the effectiveness of the trained ultrasonic perception network on the phantom's back. We first establish a static contact between the lumbar region of the phantom back and the ultrasound probe, and then the interaction force is steadily increased. Our purpose is to examine the confidence probability change in the localization of the spinous process during the procedure. The result of the trained ultrasonic network is performance in Fig. 7. The confidence probability in the spinous process position is only 0.06 when the ultrasound probe initially touches the phantom's back. When the static contact between the phantom's back and the ultrasound probe is well established, the confidence in the spinous process position increases to 0.75. It can be seen that the neural network's confidence in the location of the spinous process increases when the shadow area becomes lighter.

B. Soft Interaction Control

To evaluate the effectiveness of the proposed control strategy with soft interaction contact, we first identify the parameters in the proposed contact model. To this end, we collect experimental data from force sensors and the corresponding motion values when sliding the robot over the back of the phantom. In particular, we set different speeds ranging from low to high for the robot end-effector to track. For the determination of the friction coefficient μ, we make the probe slide over the skin at a very low speed, making the resistance force arising from deformation negligible. To identify k_1 and k_2, we specify the different interaction strengths between the ultrasound probe and the deformable skin surface under different sliding speeds, ranging from $0.2\,\mathrm{m/s}$ to $1\,\mathrm{m/s}$. The speed range here is utilized exclusively for identifying contact model parameters and is not applied to the scanning speed.

TABLE I
CONTACT MODEL PARAMETERS

μ	k_1	k_2	E^* (kPa)	R (m)
0.39	0.001	0.003	6.3	0.03

The plot of the data for model identification of soft contact model parameters is shown in Fig. 8, where the x-axis represents different sliding speeds and the y-axis represents the resistance force f_b due to deformation, which is obtained by subtracting the dry friction values from the F/T sensor readings along the movement direction. Moreover, we collect data with different interaction forces, namely $3\,\mathrm{N}$, $6\,\mathrm{N}$, $9\,\mathrm{N}$, and $12\,\mathrm{N}$, respectively. With the collected data, we subsequently employ the least squares technique for model identification to obtain the numerical values for the parameters k_1 and k_2 to best fit the contact model. The relevant values obtained upon model identification are summarized in Table I.

With the identified contact model parameters available, we use these values to set up the MPC controller. The nonlinear optimization problem in our implemented MPC controller is addressed with the help of CasADi [36]. The horizon of the MBC controller is set to predict over five steps. Our goal is to show the effectiveness of the developed contact models in terms of force-tracking tasks, which are the key factors in the quality of the spinal reconstruction results [37]. We make the robot track several given paths while each one is associated with a specified force profile over the same deformable surface, namely the step, slope, and wave forces.

For the purpose of comparison, we also implement a baseline controller that operates without incorporating a soft contact model, taking the dry friction into account only when tracking the specified references. The plot of the tracking performance for both approaches in terms of step, slope, and wave force tracking is shown in Fig. 9. It can be seen that our proposed method admits a better performance, as evidenced by the lower tracking errors compared to the baseline approach. The numerical tracking results are provided in Table II. It can be seen that our proposed controller attains better performance than the baseline controller in terms of tracking precision for both position and force tracking, thanks to the awareness of the developed soft contact model.

C. Spinal Reconstruction

Finally, we evaluate the AuSoScan platform by integrating the perception module and the control system. The acquired ultrasound images, along with their spatial information, are

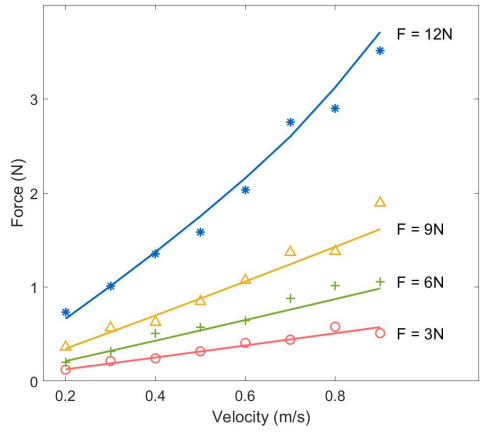

Fig. 8. Contact model identification for parameters k_1 and k_2.

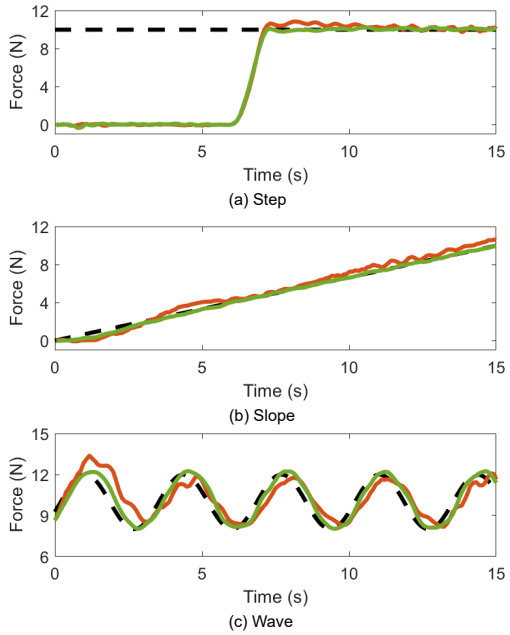

Fig. 9. Comparison of tracking different force profiles where dashed lines denote the reference, green lines represent the proposed method, and red lines denote the baseline controller.

collectively recorded for the subsequent reconstruction program to reveal the spine. The condition of the spine, i.e., the curvature angle, is then assessed with the reconstructed spinal image.

During the real experiments, we scanned a realistic phantom and a human subject from the waist to the neck. The snapshots of the real experimental procedure are shown in Fig. 11. The lateral motion of the probe is adjusted in real time based on the immediate feedback from the ultrasound images. The displacement data of the probe when scanning the phantom is shown in Fig. 10.

The acquired 3D spinal image is shown in Fig. 12. It can be observed that the acquired spinal image is clear enough to measure the curvature for a professional sonographer. By picking the most tilted vertebrae in the lower spine and the

TABLE II
TRACKING PERFORMANCE

	w/o deformation model		w/ deformation model	
	Position (cm)	Force (N)	Position (cm)	Force (N)
Step	0.97	0.357	0.53	0.106
Slope	0.83	0.393	0.39	0.185
Wave	1.51	0.959	1.02	0.535

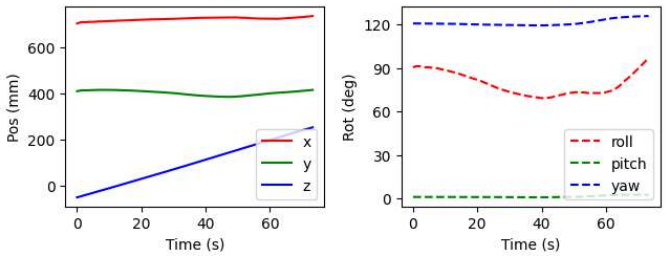

Fig. 10. Plot of the evolution of the probe movement during ultrasound scanning of the phantom.

upper spine, respectively, the curvature of the spine can be measured to be 33°, which validates the effectiveness of AuSoScan in terms of measuring spinal curvature angle for scoliosis assessment.

VI. CONCLUSION

In this paper, we presented AuSoScan, a dedicated robotic platform enabling the automatic acquisition of ultrasound images to facilitate scoliosis assessment. Mainly, AuSoScan consists of three modules: the control framework, the ultrasound image perception block, and the spinal reconstruction program. The experimental results show that AuSoScan is effective in autonomously performing ultrasound scanning.

In the current setup, there are still a few limitations. For example, there is a lack of illustrating the effectiveness of our robotic sonographer when it comes to operating under complex situations, such as severe scoliosis patients with uneven shoulders. Therefore, it will be desirable to use our robotic platform for imaging subjects with severe scoliosis symptoms.

For future work, we would like to make the robot system more compliant and reactive in terms of unexpected external disturbances [38], [39]. Moreover, the proposed approach could potentially be extended to ultrasound imaging of various organs, such as the heart, liver, kidneys, and limbs. Each organ presents unique challenges that must be addressed to optimize the imaging process. For instance, effective motion compensation is crucial for cardiac ultrasound to counteract the impacts of respiratory movements and heartbeat. The effectiveness of our soft contact-aware scanning strategy could be enhanced by adapting it to meet the specific requirements of different organs, thereby broadening its applicability and improving overall imaging performance.

CONFLICT OF INTEREST

Y. Zheng is the inventor of patents related to the 3D ultrasound imaging for scoliosis assessment, and the founder,

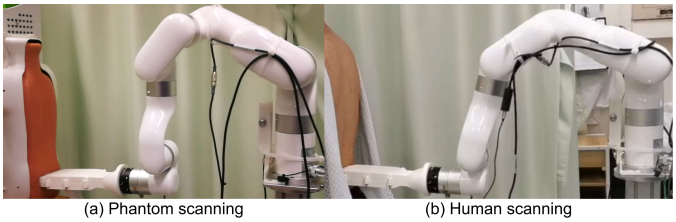

(a) Phantom scanning (b) Human scanning

Fig. 11. Procedure of ultrasonic scanning of (a) phantom and (b) human.

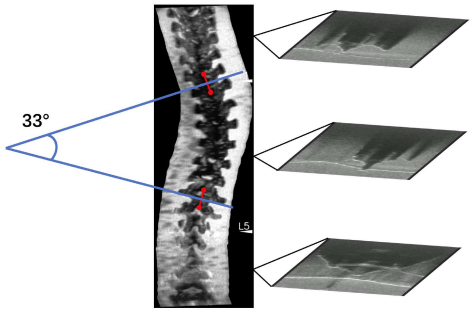

Fig. 12. Spinal reconstruction results for the phantom, where the spinal image is obtained by stacking the acquired ultrasound images layer by layer. The obtained spine is evaluated to have a curvature angle of 33°.

director, and shareholder of a startup company, Telefield Medical Imaging Limited, which manufactures Scolioscan.

REFERENCES

[1] C. J. Goldberg, D. P. Moore, E. E. Fogarty, and F. E. Dowling, "Scoliosis: a review," *Pediatric surgery international*, vol. 24, no. 2, pp. 129–144, 2008.

[2] M. R. Konieczny, H. Senyurt, and R. Krauspe, "Epidemiology of adolescent idiopathic scoliosis," *Journal of children's orthopaedics*, vol. 7, no. 1, pp. 3–9, 2013.

[3] J. Cobb, "Outline for the study of scoliosis," *American Academy of Orthopaedic Surgeons, Instructional Course Lectures*, vol. 5, pp. 261–275, 1948.

[4] J. Z. J. Lee, D. J. L. Lam, and K. B. L. Lim, "Late presentation in adolescent idiopathic scoliosis: who, why, and how often?" *Journal of Pediatric Orthopaedics B*, vol. 23, no. 1, pp. 6–14, 2014.

[5] M. S. Linet, P. Rajaraman *et al.*, "Children's exposure to diagnostic medical radiation and cancer risk: epidemiologic and dosimetric considerations," *Pediatric radiology*, vol. 39, no. 1, pp. 4–26, 2009.

[6] A. Simony, E. J. Hansen, S. B. Christensen, L. Y. Carreon, and M. O. Andersen, "Incidence of cancer in adolescent idiopathic scoliosis patients treated 25 years previously," *European Spine Journal*, vol. 25, pp. 3366–3370, 2016.

[7] P. R. Hoskins, K. Martin, and A. Thrush, *Diagnostic ultrasound: physics and equipment*. CRC Press, 2019.

[8] Y. P. Zheng and T. T. Y. Lee, "3D ultrasound imaging of the spine," in *Bone Quantitative Ultrasound*. Springer, 2022, pp. 349–372.

[9] A. Duan, M. Victorova, J. Zhao, Y. Sun, Y. Zheng, and D. Navarro-Alarcon, "Ultrasound-guided assistive robots for scoliosis assessment with optimization-based control and variable impedance," *IEEE Robotics and Automation Letters*, vol. 7, no. 3, pp. 8106–8113, 2022.

[10] H. Chen, L. Wu, Q. Dou, J. Qin, S. Li, J.-Z. Cheng, D. Ni, and P.-A. Heng, "Ultrasound standard plane detection using a composite neural network framework," *IEEE transactions on cybernetics*, vol. 47, no. 6, pp. 1576–1586, 2017.

[11] Q.-H. Huang, Z. Yang, W. Hu, L.-W. Jin, G. Wei, and X. Li, "Linear tracking for 3-d medical ultrasound imaging," *IEEE transactions on Cybernetics*, vol. 43, no. 6, pp. 1747–1754, 2013.

[12] C. Luo, Y. Chen, H. Cao, M. A. A. Sibahee, W. Xu, and J. Zhang, "Multi-modal autonomous ultrasound scanning for efficient human–machine fusion interaction," *IEEE Transactions on Automation Science and Engineering*, vol. 22, pp. 4712–4723, 2025.

[13] C. Shen, Z. Deng, J. Wang, S. Wang, and C. Chen, "Towards autonomous robotic ultrasound scanning using the reinforcement learning-based volumetric data navigation method," in *2023 WRC Symposium on Advanced Robotics and Automation (WRC SARA)*, 2023, pp. 335–340.

[14] K. Su, J. Liu, X. Ren, Y. Huo, G. Du, W. Zhao, X. Wang, B. Liang, D. Li, and P. X. Liu, "A fully autonomous robotic ultrasound system for thyroid scanning," *Nature Communications*, vol. 15, no. 1, p. 4004, 2024.

[15] D. Navarro-Alarcon, J. Qi, J. Zhu, and A. Cherubini, "A lyapunov-stable adaptive method to approximate sensorimotor models for sensor-based control," *Frontiers in Neurorobotics*, vol. 14, p. 59, 2020.

[16] D. Huang, C. Yang, M. Zhou, A. Karlas, N. Navab, and Z. Jiang, "Robot-assisted deep venous thrombosis ultrasound examination using virtual fixture," *IEEE Transactions on Automation Science and Engineering*, 2024.

[17] S. Yu, K. K. Tan, B. L. Sng, S. Li, and A. T. H. Sia, "Feature extraction and classification for ultrasound images of lumbar spine with support vector machine," in *2014 36th Annual International Conference of the IEEE Engineering in Medicine and Biology Society*. IEEE, 2014, pp. 4659–4662.

[18] P. Chatelain, A. Krupa, and N. Navab, "Confidence-driven control of an ultrasound probe," *IEEE Transactions on Robotics*, vol. 33, no. 6, pp. 1410–1424, 2017.

[19] K. He, X. Zhang, S. Ren, and J. Sun, "Deep residual learning for image recognition," in *Proceedings of the IEEE conference on computer vision and pattern recognition*, 2016, pp. 770–778.

[20] H. Huang, C. Yang, and C. L. P. Chen, "Optimal robot–environment interaction under broad fuzzy neural adaptive control," *IEEE Transactions on Cybernetics*, vol. 51, no. 7, pp. 3824–3835, 2021.

[21] L. Hu, A. Duan, M. Li, A. Cherubini, L. Li, and D. Navarro-Alarcon, "Paint with the sun: A thermal-vision guided robot to harness solar energy for heliography," *IEEE Sensors Journal*, vol. 22, no. 18, pp. 18 130–18 142, 2022.

[22] M. Muddassir, G. Limbert, B. Zhang, A. Duan, J.-J. Tan, and D. Navarro-Alarcon, "Model predictive thermal dose control of a robotic laser system to automate skin photorejuvenation," *IEEE/ASME transactions on mechatronics*, vol. 28, no. 2, pp. 737–747, 2022.

[23] A. Duan, S. Huo, H.-Y. Lee, P. Zhou, J. G. Romero, C. Yang, and D. Navarro-Alarcon, "Robust grasping by bimanual robots with stable parameterization-based contact servoing," *IEEE/ASME Transactions on Mechatronics*, pp. 1–12, 2024.

[24] D. Navarro-Alarcon, S. Singh, T. Zhang, H. L. Chung, K. W. Ng, M. K. Chow, and Y. Liu, "Developing a compact robotic needle driver for mri-guided breast biopsy in tight environments," *IEEE Robotics and Automation Letters*, vol. 2, no. 3, pp. 1648–1655, 2017.

[25] F. Zhong, Y. Wang, Z. Wang, and Y.-H. Liu, "Dual-arm robotic needle insertion with active tissue deformation for autonomous suturing," *IEEE Robotics and Automation Letters*, vol. 4, no. 3, pp. 2669–2676, 2019.

[26] L. Han, H. Wang, Z. Liu, W. Chen, and X. Zhang, "Vision-based cutting control of deformable objects with surface tracking," *IEEE/ASME Transactions on Mechatronics*, vol. 26, no. 4, pp. 2016–2026, 2020.

[27] Q. Sheng, Z. Geng, L. Hua, and X. Sheng, "Hybrid vision-force robot force control for tasks on soft tissues," in *2021 27th International Conference on Mechatronics and Machine Vision in Practice (M2VIP)*. IEEE, 2021, pp. 705–710.

[28] L. Wijayarathne, Q. Sima, Z. Zhou, Y. Zhao, and F. L. Hammond, "Simultaneous trajectory optimization and force control with soft contact mechanics," in *2020 IEEE/RSJ International Conference on Intelligent Robots and Systems (IROS)*. IEEE, 2020, pp. 3164–3171.

[29] Y.-P. Zheng, T. T.-Y. Lee, K. K.-L. Lai, B. H.-K. Yip, G.-Q. Zhou, W.-W. Jiang, J. C.-W. Cheung, M.-S. Wong, B. K.-W. Ng, J. C.-Y. Cheng *et al.*, "A reliability and validity study for scolioscan: a radiation-free scoliosis assessment system using 3D ultrasound imaging," *Scoliosis and spinal disorders*, vol. 11, no. 1, pp. 1–15, 2016.

[30] M. Victorova, D. Navarro-Alarcon, and Y.-P. Zheng, "3D ultrasound imaging of scoliosis with force-sensitive robotic scanning," in *2019 Third IEEE International Conference on Robotic Computing (IRC)*, 2019, pp. 262–265.

[31] Y. Yuan, L. Guo, and H. Liu, "Model predictive cooperative control with ism for multiagent systems under stochastic communication protocol," *IEEE Transactions on Cybernetics*, vol. 51, no. 12, pp. 6004–6016, 2021.

[32] T. Gold, A. Völz, and K. Graichen, "Model predictive position and force trajectory tracking control for robot-environment interaction," in *2020 IEEE/RSJ International Conference on Intelligent Robots and Systems (IROS)*. IEEE, 2020, pp. 7397–7402.

[33] G. Duchemin, P. Maillet, P. Poignet, E. Dombre, and F. Pierrot, "A hybrid position/force control approach for identification of deformation models

of skin and underlying tissues," *IEEE Transactions on Biomedical Engineering*, vol. 52, no. 2, pp. 160–170, 2005.
[34] V. L. Popov *et al.*, *Contact mechanics and friction*. Springer, 2010.
[35] C.-W. J. Cheung, G.-Q. Zhou, S.-Y. Law, T.-M. Mak, K.-L. Lai, and Y.-P. Zheng, "Ultrasound volume projection imaging for assessment of scoliosis," *IEEE transactions on medical imaging*, vol. 34, no. 8, pp. 1760–1768, 2015.
[36] J. A. Andersson, J. Gillis, G. Horn, J. B. Rawlings, and M. Diehl, "CasADi: a software framework for nonlinear optimization and optimal control," *Mathematical Programming Computation*, vol. 11, pp. 1–36, 2019.
[37] A. Duan, C. Yang, J. Zhao, S. Huo, P. Zhou, W. Ma, Y. Zheng, and D. Navarro-Alarcon, "Safe learning by constraint-aware policy optimization for robotic ultrasound imaging," *IEEE Transactions on Automation Science and Engineering*, 2024.
[38] P. Zhou, P. Zheng, J. Qi, C. Li, A. Duan, M. Xu, V. Wu, and D. Navarro-Alarcon, "Neural reactive path planning with Riemannian motion policies for robotic silicone sealing," *Robotics and Computer-Integrated Manufacturing*, vol. 81, p. 102518, 2023.
[39] W. Ma, A. Duan, H.-Y. Lee, P. Zheng, and D. Navarro-Alarcon, "Human-aware reactive task planning of sequential robotic manipulation tasks," *IEEE Transactions on Industrial Informatics*, vol. 21, no. 4, pp. 2898–2907, 2025.

Anqing Duan received his Ph.D. degree in robotics from the Italian Institute of Technology (IIT) and the University of Genoa (UniGe), Italy, in 2021. He was a Research Associate at The Hong Kong Polytechnic University (PolyU). He is currently a Visiting Assistant Professor with the Robotics Department at Mohamed Bin Zayed University of Artificial Intelligence (MBZUAI). His research interests include robot learning and control with a focus on human-centered and healthcare robotic applications.

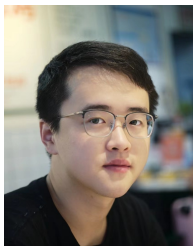

Wanli Liuchen received the B.Eng. in Mechanical Engineering and Automation from the China University of Petroleum (Beijing) in 2022 and completed the M.Sc. in Mechanical Engineering at The Hong Kong Polytechnic University in 2024. He is currently a Research Assistant at the ROMI Lab, The Hong Kong Polytechnic University, where his work focuses on robotic systems, particularly in the field of medical robotics. His research interests include robot navigation, machine learning, and healthcare robotics applications.

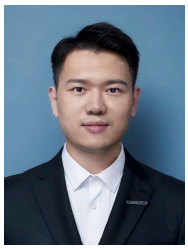

Peng Zhou received his Ph.D. degree in robotics from The Hong Kong Polytechnic University, Hong Kong SAR, in 2022. In 2021, he was a Visiting Researcher at the Robotics, Perception, and Learning Lab, KTH Royal Institute of Technology, Stockholm, Sweden. From 2022 to 2024, he was a Postdoctoral Research Fellow at the Department of Computer Science, The University of Hong Kong. He is currently an Assistant Professor at the School of Advanced Engineering, Great Bay University (GBU). His research interests include deformable object manipulation, robotic perception and learning, and task and motion planning.

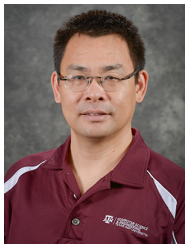

Dezhen Song (Senior Member, IEEE)) received the B.S. and M.S. degrees from Zhejiang University, Hangzhou, China, in 1995 and 1998, respectively, and the Ph.D. degree from the University of California at Berkeley, Berkeley, in 2004. From 2004 to 2023, He was a Professor with Department of Computer Science and Engineering, Texas A&M University, College Station, USA. He is currently a Professor and an Deputy Department Head with the Department of Robotics, Mohamed Bin Zayed University (MBZUAI), Abu Dhabi, United Arab Emirates.

His primary research interests include robot perception, networked robotics, visual navigation, agricultural robotics, and automation. Dr. Song received the Kayamori Best Paper Award of the 2005 IEEE International Conference on Robotics and Automation (with J. Yi and S. Ding). He received the Faculty Early Career Development (CAREER) Award from US NSF in 2007, Amazon Research Award in 2020. From 2008 to 2012, he was an Associate Editor of IEEE TRANSACTIONS ON ROBOTICS (T-RO). From 2010 to 2014, he was an Associate Editor of IEEE TRANSACTIONS ON AUTOMATION SCIENCE AND ENGINEERING (T-ASE). From 2017 to 2020, he was a Senior Editor for IEEE ROBOTICS AND AUTOMATION LETTERS (RA-L). He is currently a Senior Editor for T-ASE.

Chenguang Yang (Fellow, IEEE) received the B.Eng. degree in measurement and control from Northwestern Polytechnical University, Xian, China, in 2005, and the Ph.D. degree in control engineering from the National University of Singapore, Singapore, in 2010. He performed postdoctoral studies in human robotics at the Imperial College London, London, U.K from 2009 to 2010. Professor Yang holds the Chair in Robotics with Department of Computer Science, University of Liverpool, UK. He is leading the Robotics and Autonomous Systems Group. He was leading Robot Teleoperation Group at Bristol Robotics Laboratory. He is a member of European Academy of Sciences and Arts (EASA). He was awarded UK EPSRC UKRI Innovation Fellowship and individual EU Marie Curie International Incoming Fellowship. He was President of Chinese Automation and Computing Society in the UK. He is the Corresponding Co-Chair of IEEE Technical Committee on Collaborative Automation for Flexible Manufacturing. As the lead author, he won the IEEE TRANSACTIONS ON ROBOTICS Best Paper Award (2012) and IEEE TRANSACTIONS ON NEURAL NETWORKS AND LEARNING SYSTEMS Outstanding Paper Award (2022). His research interest lies in robot control and learning, human-robot interaction, and intelligent system design.

Yongping Zheng (Senior Member, IEEE) received the B.Sc. and M.Eng. degrees in electronics and information engineering from the University of Science and Technology of China, and the Ph.D. degree in biomedical engineering from The Hong Kong Polytechnic University (PolyU), Hong Kong, in 1997.

After a postdoctoral fellowship at the University of Windsor, Canada, he joined PolyU as an Assistant Professor and was promoted to Professor, in 2008, and Chair Professor, in 2019. In July 2017, he was appointed as the Henry G. Leong Professor in biomedical engineering. He is currently the Director of the Jockey Club Smart Ageing Hub, and the Research Institute for Smart Ageing, PolyU. His main research interests include biomedical ultrasound instrumentation, soft tissue elasticity measurement and imaging, 3D ultrasound imaging, ultrasound assessment of musculoskeletal tissues, ultrasound image and signal processing, and smart aging technologies.

Prof. Zheng is a fellow of The Hong Kong Institution of Engineers (HK), a Secretary of the World Association of Chinese Biomedical Engineers, from 2017 to 2019, the Past Chair of the Biomedical Engineering Division, HKIE, and an Honorary Advisor of the Hong Kong Medical and Healthcare Device Industry Association (HMHDIA). He serves as the President for the Guangdong Hong Kong Macau Chapter of the International Society of Gerontechnology.

David Navarro-Alarcon (Senior Member, IEEE) received his Ph.D. degree in mechanical and automation engineering from The Chinese University of Hong Kong (CUHK), Hong Kong, in 2014. From 2015 to 2017, he was a Research Assistant Professor at the CUHK T Stone Robotics Institute. Since 2017, he has been with The Hong Kong Polytechnic University (PolyU), Hong Kong, where he is currently an Associate Professor of Robotics in the Department of Mechanical Engineering. His current research interests include perceptual robotics and control theory. Dr. Navarro-Alarcon currently serves as an Associate Editor of the IEEE TRANSACTIONS ON ROBOTICS.